TUMOR IMMUNOLOGY AND MICROENVIRONMENT

INTERNATIONAL
JOURNAL of CANCER

Reversing vemurafenib-resistance in primary melanoma cells by combined romidepsin and type I IFN treatment through blocking of tumorigenic signals and induction of immunogenic effects

Alessandra Fragale[1] | Emilia Stellacci[1] | Giulia Romagnoli[1] | Valerio Licursi[2] |
Stefania Parlato[1] | Irene Canini[1] | Giacomo Remedi[1] | Maria Buoncervello[3] |
Paola Matarrese[4] | Lucia Pedace[5] | Barbara Ascione[4] | Simone Pizzi[6] |
Marco Tartaglia[6] | Stefania D'Atri[7] | Carlo Presutti[8] | Imerio Capone[1] |
Lucia Gabriele[1]

[1]Department of Oncology and Molecular Medicine, Istituto Superiore di Sanità (ISS), Rome, Italy

[2]Institute of Molecular Biology and Pathology (IBPM), National Research Council (CNR) of Italy, Rome, Italy

[3]Research Coordination and Support Service, ISS, Rome, Italy

[4]Center for Gender-Specific Medicine, ISS, Rome, Italy

[5]Department of Pediatric Haematology/Oncology, Cell and Gene Therapy, Ospedale Pediatrico Bambino Gesù, IRCCS, Rome, Italy

[6]Molecular Genetics and Functional Genomics, Ospedale Pediatrico Bambino Gesù, IRCCS, Rome, Italy

[7]Molecular Oncology Laboratory, Istituto Dermatopatico dell'Immacolata IDI-IRCCS, Rome, Italy

[8]Department of Biology and Biotechnology "Charles Darwin", Sapienza University, Rome, Italy

Correspondence
Lucia Gabriele and Alessandra Fragale, Department of Oncology and Molecular Medicine, Istituto Superiore di Sanità (ISS), viale Regina Elena 299, 00161 Rome, Italy.
Email: lucia.gabriele@iss.it and alessandra.fragale@iss.it

Abstract

BRAF^{V600} mutations are the most common oncogenic alterations in melanoma cells, supporting proliferation, invasion, metastasis and immune evasion. In patients, these aberrantly activated cellular pathways are inhibited by BRAFi whose potent antitumor effect and therapeutic potential are dampened by the development of resistance. Here, by using primary melanoma cell lines, generated from lymph node lesions of metastatic patients, we show that the combination of two FDA-approved drugs, the histone deacetylate inhibitor (HDCAi) romidepsin and the immunomodulatory agent IFN-α2b, reduces melanoma proliferation, long-term survival and invasiveness and overcomes acquired resistance to the BRAFi vemurafenib (VEM). Targeted resequencing revealed that each VEM-resistant melanoma cell line and the parental counterpart are characterized by a distinctive and similar genetic fingerprint, shaping the differential and specific antitumor modulation of MAPK/AKT pathways by combined

Abbreviations: DCs, dendritic cells; HDAC, histone deacetylase; IFN, interferon; IRF-1, interferon regulatory factor-1; MM, metastatic melanoma; MM-R, metastatic melanoma resistant; RNAseq, RNA sequencing; PD-L1, programmed death ligand-1; TME, tumor microenvironment; VEM, vemurafenib.

drug treatment. By using RNA-sequencing and functional in vitro assays, we further report that romidepsin-IFN-α2b treatment restores epigenetically silenced immune signals, modulates MITF and AXL expression and induces both apoptosis and necroptosis in sensitive and VEM-resistant primary melanoma cells. Moreover, the immunogenic potential of drug-treated VEM-resistant melanoma cells results significantly enhanced, given the increased phagocytosis rate of these cells by dendritic cells, which in turn exhibit also a selective down-modulation of the immune checkpoint TIM-3. Overall, our results provide evidence that combined epigenetic-immune drugs can overcome VEM resistance of primary melanoma cells by oncogenic and immune pathways reprogramming, and pave the way for rapidly exploiting this combination to improve BRAFi-resistant metastatic melanoma treatment, also via reinforcement of immune checkpoint inhibitor therapy.

What's new?
Melanoma cells often have BRAF[V600] mutations, which promote proliferation and metastasis. While BRAF inhibitors have potent antitumor effects, patients eventually develop resistance. Here, the authors show that in melanoma cell lines derived from metastatic patients, the combination of two FDA-approved drugs, a histone deacetylate inhibitor and an immunomodulatory drug, overcame resistance to the BRAF inhibitor vemurafenib. They also describe a distinct genetic fingerprint associated with vemurafenib resistance. Further developing this combination approach of epigenetic + immune drugs could lead to better outcomes for patients with melanoma resistant to BRAF inhibitors.

1 | INTRODUCTION

Melanoma is a heterogeneous tumor characterized by an ensemble of dysregulated signal pathways resulting in the acquisition of tumoral traits supporting cancer progression throughout a dynamic adaptation to tumor microenvironment (TME) changes.[1] The BRAF kinase is the target of a narrow spectrum of activating point mutations, mostly the substitution BRAF[V600E] occurring in 40% to 50% of all melanomas, leading to the constitutive activation of MAPK and associated with poor outcome. Drugs blocking the MAPK cascade have drastically improved the survival rate of a significant proportion of patients, but this success is hampered by emergence of drug resistance involving MAPK signaling reactivation or other proliferative and survival pathways, such as PI3K-AKT-mTOR.[2] Acquired drug resistance is also driven by other elements, such as epigenetic events supporting the prevalence of slow-cycling cancer cells.[3] Finally, BRAFi resistance is also influenced by TME inflammation, sustaining melanoma phenotypic switch and functional alterations of immune populations.[4,5]

A master regulator of melanoma cell plasticity is MITF, which regulates the expression of genes driving the melanoma phenotypic switch. High MITF expression levels lead to the predominance of a proliferative and weakly invasive cellular state, whereas low MITF expression associates with highly invasive and less proliferative phenotype. Although drug-resistant melanoma cells mostly show low expression of MITF, BRAFi may lead to increased expression of MITF associated with resistance observed in more than 20% of melanomas. In addition, melanoma resistance may lead to the emergence of slow-cycling tumor cells enriched in receptor tyrosine kinases, such as AXL, providing survival signals independently from MAPK signaling.[6] Nevertheless, MITF[low]/AXL[high] status has been considered as one of the most prominent marker of resistance.[7] Noteworthy, the MITF/AXL-mediated phenotypic switch is outlined by distinct epigenetic signatures.[8]

BRAF-driven tumorigenesis and the emergence of resistance to BRAFi are phenomena associated with dysregulation of histone-modifying enzymes, such as HDACs.[9] Accordingly, drug-resistant melanoma cells exposed to the HDACi vorinostat were found to undergo apoptotic death associated to elevated ROS levels in BRAF[V600E] melanoma patients that had progressed on BRAFi therapy, resulting in a selective ablation of drug-resistant tumor cells.[10,11] The HDACi panobinostat was reported to restore BRAFi sensitivity of melanoma cells.[12] Of interest, in soft tissue sarcoma the HDACi chidamide significantly increases PD-L1 expression and synergizes with anti-PD-1 in promoting tumor regression and improving survival.[13]

The selective HDAC1/2 inhibitor romidepsin, a drug approved in cutaneous and peripheral T cell lymphomas, induces cell cycle arrest and apoptosis in solid tumors.[14] Romidepsin is effective in the nanomolar range to induce radiosensitizing effects in lung and bladder

tumors, and in combination with mTOR inhibition has been reported to be effective against uveal melanoma.[15,16] Recent reports highlighted the immunomodulatory properties of romidepsin, including the regulation of PD-L1 expression, associated to modulation of antitumor effects in solid tumors.[17]

In our study, we sought to evaluate whether the combination of romidepsin with IFN-α2b, an immunomodulatory cytokine widely used in the past for melanoma treatment[18] could exert antitumor and immunogenic activity against BRAF-mutated melanoma and BRAFi acquired resistance. To this end, we used primary BRAF^V600E/R melanoma cells derived from metastatic lesions and we generated in vitro their vemurafenib (VEM)-resistant counterparts. We found that the romidepsin-IFN combined treatment owns a high capability to inhibit melanoma invasiveness, and to induce mixed apoptotic/necroptotic cell death in both *BRAF* mutated and VEM-resistant cells, inhibiting their metastatic potential and reversing BRAFi resistance along with remarkable inhibition of MITF and AXL signatures. Moreover, this treatment enhances the immunogenic potential of drug-treated VEM-resistant melanoma cells whose increased rate of phagocytosis by dendritic cells (DCs) that in turn show a selective down-modulation of TIM-3.

2 | MATERIALS AND METHODS

2.1 | Cells

Primary melanoma cells used in our study were previously established at IDI-IRCCS from patient metastases. Cells were renamed as Metastatic Melanoma (MM)1, MM2, MM3, MM4, MM5 and MM6 cells.[19,20] MM cells were cultured in RPMI 1640 (Gibco) supplemented with 10% FBS; SK-MEL-28 (RRID:CVCL_0526) cells were purchased from the ATCC (Rockville, MD). Monocytes were freshly isolated from PBMCs from healthy donors by using CD14 microbeads (Miltenyi Biotec), and then cultured in presence of GM-CSF (50 ng/mL; PeproTech) and IL4 (500 U/mL; R&D Systems), as previously described to obtain IL4-DCs.[21] After 5 days, DCs were collected and used for phagocytosis assays or treated for further 24 hours with Romidepsin, IFN or both as described.[21] All experiments were performed with mycoplasma-free cells.

2.2 | BRAF mutation scan and STR

Mutation scanning of the entire coding sequence of *BRAF* was performed by Sanger sequencing in all cell lines using an ABI Prism 3500 Genetic Analyzers (Applied Biosystems) and the ABI BigDye Terminator Sequencing Kit V.3.1 (Applied Biosystems). All human cell lines have been authenticated using short tandem repeat (STR) profiling within the last 3 years. MM cells were authenticated by STR for evaluation of identity comparing all primary cell lines and parental derivative tissues with AmpF𝓁STR Identifiler PCR Amplification Kit (ThermoFisher) within the last 3 years.

2.3 | Cell viability

Cell viability assay was performed by CellTiter 96 AQueous Cell Proliferation Assay (Promega) to determine cytotoxicity effects after drug treatment, using DMSO as vehicle control. Briefly, 4×10^3 cells were seeded on a 96-well plate and were treated the following day with romidepsin, IFN or combination for 24, 48 and 72 hours. At the end of treatments, cell viability was detected, upon MTS reagent addition, on a VICTOR3 Plate Reader (PerkinElmer). Each experimental condition was performed in triplicate and repeated at least twice.

2.4 | Generation of BRAFi-resistant cell lines (MM-R) and drugs

To generate vemurafenib (PLX4032, Sellekchem; VEM) resistant MM1-R, MM2-R and MM3-R, BRAF^V600 parental cells were selected by low-density seeding growth in medium containing increased VEM concentrations, ranging from 0.1 to 5 μM until appearance of resistant clones within 4 to 6 weeks subsequent. The viable cells at the higher concentrations of VEM were expanded for several weeks and frozen till further use. Romidepsin (or FK228, or depsipeptide or Istodax) was purchased from Selleckchem; IFN-α2b (IntronA) from MSD. Concentrations used are reported in Table S1.

2.5 | Western blotting

Total proteins extracts were analyzed as described.[21] Nitrocellulose was incubated with antibodies Phospho-MAPK 9106, Phospho-AKT 9271, Phospho-MLKL Cat. 37333 and RIP 3493 (Cell Signaling Technology); Bcl-2 SC-509, PD-L1 sc-293 425 and GAPDH sc-47 724 (Santa Cruz Biotechnology); c-Myc 13-2500 (ThermoFisher).

2.6 | Real-time quantitative PCR

Total RNA was extracted from cells using the Total RNA Purification PLUS Kit (NORGEN Biotek Corp.) and reverse transcribed.[21] Quantitative PCR (qPCR) was performed in duplicate by using SensiFAST-SYBR (Bioline) and LightCycler 480 System (Roche Diagnostics). Values were normalized respect to HPRT gene. Sequences of primers used for real-time PCR are reported in Table S2.

2.7 | Wound healing assay

Cells were seeded to confluence in 12-well plates, and a wound was made in the center of the cell monolayer using a sterile 200-μL pipette tip. The monolayer was rinsed three times with PBS and placed in drug-treated RPMI-1640 complete medium. Phase contrast images were captured after 24 hours and a digital image of the scar was captured at a magnification of ×10 (Leica, DMI6000).

2.8 | Clonogenic assay

Clonogenic ability of cells was performed by seeding 4×10^3 cells in a 6-well plate. After 24 hours, cells were treated with drugs and assayed by long-term colony formation assays in the absence and presence of drugs for 15 days. At day 15 of culture, media were removed, and then the cells were washed with PBS, fixed and stained with 2% crystal violet and imaged on ChemiDoc image system (Bio-Rad Laboratories).

2.9 | Flow cytometry analyses

2.9.1 | Cell death

Quantitative evaluation of cell death was performed by flow cytometry after double cell staining by using FITC-conjugated AnnexinV (AV) and 5 μg/mL Propidium iodide (PI) 10 minutes at room temperature (Marine Biological Laboratory). To study the effect of specific death inhibitors cells were treated with 10 μM z-VAD-FMK or 100 μM Necrostatin-1 (Enzo LifeSciences). Results were reported as percentage of dead cells (AV/PI double positive + AV single positive + PI single positive). At the end of incubation time, samples were immediately analyzed.

2.9.2 | Mitochondrial ROS production

At the end of drug treatments, cells (5×10^4) were incubated with 5 μM MitoSOX (Red Mitochondrial Superoxide Indicator, Thermo-Fisher) in complete medium, for 30 minutes at 37°C, washed in PBS and immediately analyzed. Quantification of mitochondrial ROS was obtained by using the median fluorescence intensity of the cytometer curves. Cell samples were washed twice in PBS and immediately analyzed.

2.9.3 | Quantitative evaluation of proteins

Cells (2×10^5) were fixed with 4% paraformaldehyde (Carlo Erba) and then permeabilized by 0.5% Triton X-100 (Sigma-Aldrich). Cells were then incubated for 1 hour at 4°C with a FITC-conjugated anti-Bcl-2 (Dako, Clone 124). After washings, cells were incubated with a MAb antibody to the active form of Bax (BD Biosciences) for 1 hour at 4°C. After washings, cells were incubated for 30 minutes at 37°C with an antimouse antibody conjugated with Cy5 (Abcam). Cell samples were washed twice in PBS and immediately analyzed.

All samples were acquired and analyzed using a FACS Calibur (BD Biosciences) equipped with a 488 nm argon laser and with a 635 nm red diode laser. At least 20 000 events/sample were acquired and analyzed using the CellQuest Pro software (BD Biosciences). In all

our cytofluorimetry experiments performed, the median fluorescence value of the isotype control was subtracted from the median fluorescence value of the corresponding positive sample (in the case of Bcl-2 and BAX proteins quantified using specific antibodies) or with the corresponding blank control (autofluorescence) in the case of fluorescent dyes (ie, MitoSox for the quantification of mitochondrial ROS production).

2.10 | Targeted resequencing and data analysis

DNA samples were analyzed using a custom panel of 554 genes implicated in cancer development and progression (Table S3) using the NimbleGen SeqCap probe hybridization kit (Roche NimbleGen). Libraries were analyzed by 150-bp paired-end sequencing on an Illumina NextSeq550 platform (Illumina). Raw data were processed and analyzed using an in-house pipeline based on the GATK Best Practices.[22,23] The UCSC GRCh37/hg19 version of genome assembly was used as reference for reads alignment by means of BWA-MEM v0.7.17 aligner. Both germline and somatic variant calling was performed giving BAM files by means of HaplotypeCaller and muTect2 algorithms (GATK v3.8), respectively, SnpEff v.4.3 and dbNSFP v.3.5 tools were used for known disease variants annotation (ClinVar), variant functional annotation, as well as for in silico prediction of impact by means of Combined Annotation Dependent Depletion (CADD) v.1.4, Mendelian Clinically Applicable Pathogenicity (M-CAP) v.1.3 and Intervar v.2.0.1. Population frequencies were annotated from both gnomAD database and in-house database, which includes ~2500 exomes. Specific filters were applied to narrow the analysis on high-quality variants (GATK hard-filtering, QUAL>100), low-frequency (gnomAD MAF <0.1%, in-house exomes database<1%) nonsynonymous SNV and INDELs within coding exons and splice regions.[23] Variants affecting the coding sequence or located within splice regions were filtered using the following criteria: quality >150; variant: reference allele ratio >15%; MAF <0.001 in public (gnomAD) and <0.01 in-house (2500 exomes) databases; CADD score >20. Only variants likely pathogenic or pathogenic were considered. The sequencing coverage and quality statistics for each sample are summarized in Table S4.

2.11 | mRNA-seq analysis

RNA-seq libraries preparation and sequencing will be performed by TIGEM using the QuantSeq 3′ mRNA-Seq Library Prep Kit FWD for Illumina using total RNA, according to manufacturer's instructions. The final libraries for single-read sequencing of 101 base pairs were carried out on an Illumina HiSeq2000. Reads quality was evaluated using FastQC (version 0.11.2, Babraham Institute, UK) tool and will be trimmed using TrimGalore software to remove adapter and low-quality bases (Q < 20). Then reads were mapped to the human Ensembl GRCh38 build reference genome using STAR version 2.5.0a

using Gene annotations corresponding to the Ensembl annotation release 99, which was used to build a transcriptome index and provided to STAR during the alignment.[24] The gene annotations were used to quantify the gene-level read counts using HTSeq-count version 0.8.0 script.[25] Subsequently, the transcript data normalization and differential gene expression (DEG) analysis were performed using Bioconductor R package RUVSeq version 1.28 and edgeR version 3.36.[26] To identify DEGs, data were filtered to remove from the analysis the genes having <1 counts per million in <6 out of 12 total samples for each comparison. Volcano plots were created using Bioconductor R package EnhancedVolcano version 1.12.0. Heatmap and hierarchical clustering were created with the R package *pheatmap* version 1.0.12. The sequencing coverage and quality statistics for each sample are summarized in Table S4.

2.12 | Gene set enrichment analysis

DEGs and gene signature were clustered by functional annotation in GO and pathway enrichment analysis using Bioconductor R package clusterProfiler version 4.2.0 with annotation of Gene Ontology Database.[27] BROAD Institute gene set enrichment analysis (GSEA) was used to assess the enrichment of the ranked DEG list vs the curated "Hallmark" gene set collections from the BROAD Molecular Signatures Database version 7.4.1.

2.13 | Phagocytosis of drug-treated MM cells by DCs

For phagocytosis quantification, BRAF^{V600} MM and MM-R cells were stained with PKH-26 Fluorescent Cell Linker (Sigma-Aldrich), and then treated with romidepsin and IFN, in combination or alone, or left untreated for 48 hours. PKH-26-labeled cells dying floating cells were harvested and incubated with DCs at 1:2 ratio in conic 15 mL tubes at 37°C for 4 hours. Afterward, cells were collected, stained with anti-CD11c-FITC (BD Biosciences) or anti-HLA-DR-PacificOrange (Thermofisher) and anti-TIM-3-PE CF594 (BD Biosciences) mAbs and analyzed by Kaluza flow cytometry and software (Beckman Coulter). The rate of phagocytosis of apoptotic melanoma cells by DCs was determined by calculating the percentage of PKH26-apo$^+$CD11c$^+$ or PKH26-apo$^+$HLA-DR$^+$ cells that were subsequently evaluated for TIM-3 expression.

2.14 | Statistical analysis

Each experiment was repeated at least three times, yielding comparable results. GraphPad Prism v.5.03 (La Jolla, CA) and Microsoft Excel were used to graph the data as mean ± SD and to calculate *P*-values using the two-tailed unpaired Student's *t*-test. In all experiments, *P*-value ≤.05 was considered as statistically significant.

3 | RESULTS

3.1 | Romidepsin and IFN-α2b in combination control the proliferation and invasiveness of primary BRAF-mutated melanoma cells

Six primary melanoma cell lines (ie, MM1, MM2, MM3, MM4, MM5 and MM6), were previously established in vitro from metastatic tissues of melanoma patients.[19,20] *BRAF* missense change affecting the recurrently mutated Val600 residue was identified in three out of the six MM cell lines. Specifically, MM1 and MM2 were found to carry BRAF^{V600E} substitution, whereas MM3 cells exhibited a valine-to-arginine (V600R) substitution, which represents ∼3% to 7% of all somatic *BRAF* mutations and preserves response to BRAFi treatment (Figure 1A). MM4, MM5 and MM6 cells were found BRAF^{WT}. The basal proliferation index of *BRAF*-mutated and WT MM cell lines was assayed, showing that MM1 and MM2 cells had a lower proliferation index over 72 hours than MM3, BRAF^{WT} and SK-Mel-28 cells (Figure 1B).

Sensitivity of BRAF^{V600} and BRAF^{WT} cells to increasing doses of romidepsin was tested to evaluate antiproliferative effects. While a dose- and time-dependent reduction in cell viability by romidepsin treatment was observed in all melanoma cells (not shown), BRAF^{V600R} MM3 and BRAF^{WT} MM4, MM5 and MM6 cells exhibited significantly higher sensitivity to this drug after 48 hours (Figure S1). IC20 romidepsin dose after 48 hours treatment was chosen for each cell line (Figure S1, Table S1). As expected, higher IC20 values of romidepsin were found for BRAF^{V600E} MM1 and MM2, suggesting an intrinsic lower sensitivity with respect to BRAF^{V600R} MM3 and BRAF^{WT} cells (Figure S1, Table S1). Of note, all MM exhibited very low dose/time-dependent inhibition of proliferation following IFN exposure at doses ranging from 10^3 to 10^5 UI/mL up to 72 hours; hence it was used at 10^4 UI/mL according to our previous works (not shown).[21,28]

Next, MM cells were tested for the antiproliferative effects of romidepsin and IFN, as monotreatment or in combination. Romidepsin induced a significant reduction of cell viability, which was further decreased in combination with IFN after 48 hours in all MM cells, underlying the lack of association with *BRAF* mutational status, although BRAF^{V600R} MM3 cells displayed the highest drug susceptibility (Figure 1C). The cell vitality decrease was further confirmed by observation of plate-detached nonviable cells vs attached viable cells with bright nucleus and intact structure (Figure S2A), and by long-term clonogenic assay showing the high potential of romidepsin and to a large extent, combined romidepsin-IFN in limiting clonogenic proliferation of both BRAF^{V600} and BRAF^{WT} MM cells (Figure S2B). Lastly, romidepsin-IFN combination exhibited strong capability to limit wound healing closure of both BRAF^{V600} and BRAF^{WT} MM cells (Figure 1D). In particular, low proliferating MM1 and MM2 cells exhibited early inhibition with respect to high proliferating MM3 and MM4 ones. These data support the capability of combined romidepsin/IFN to limit the proliferative and invasive potential of melanoma cells that were further evaluated for the *MITF/AXL* status. BRAF^{V600E} MM1 and MM2 cells exhibited basally high *AXL* and undetectable *MITF*
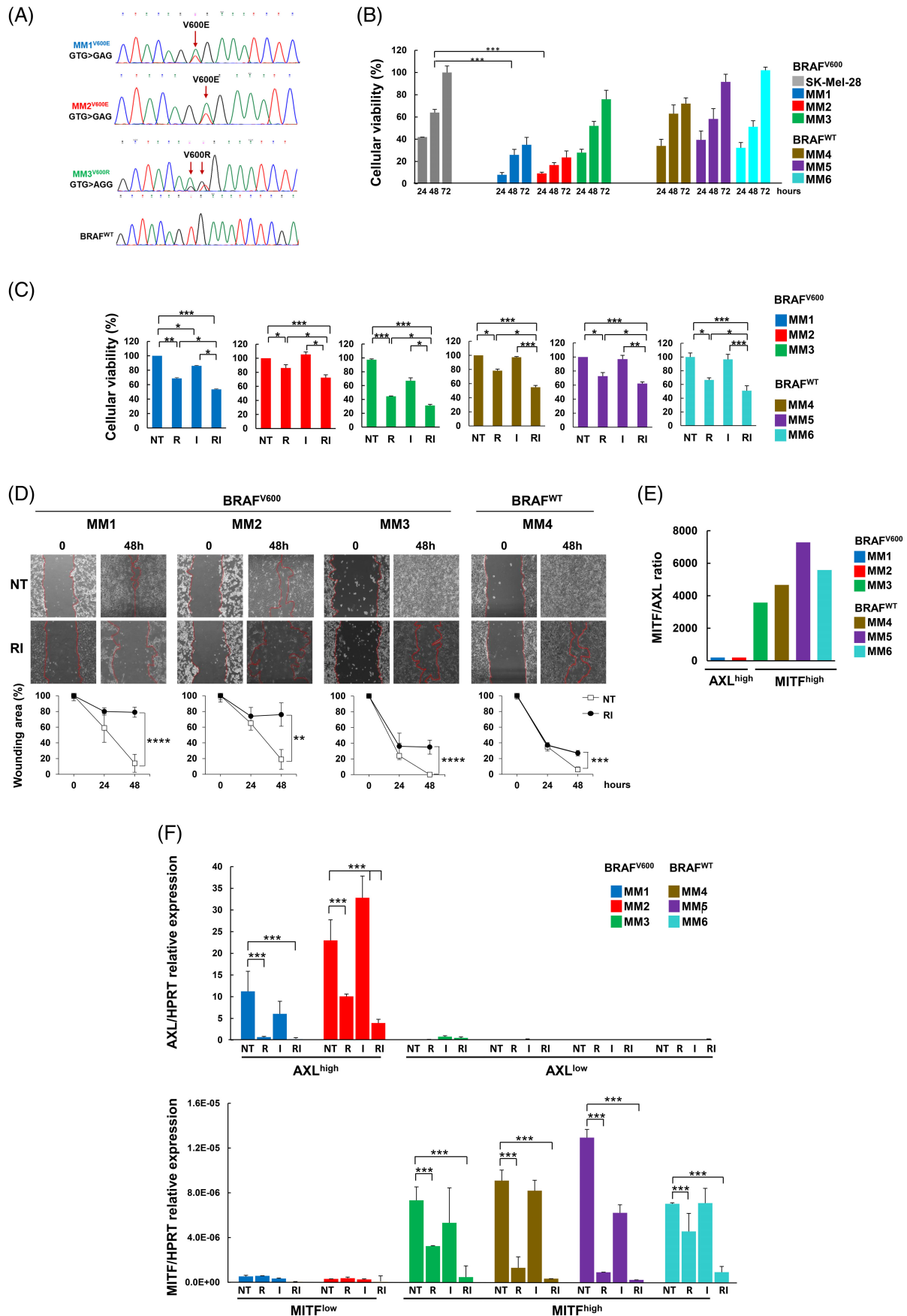
FIGURE 1 Legend on next page.

expression levels (low *MITF/AXL* ratio), whereas BRAF^V600R MM3 and BRAF^WT cells were found to express high levels of *MITF* and barely detectable levels of *AXL* (high *MITF/AXL* ratio; Figure 1E). Therefore, we adopted also AXL^high MM1, AXL^high MM2 and MITF^high MM3 designation. Remarkably, upon IFN/romidepsin, or single romidepsin treatment the high expression of *MITF* and *AXL* in the respective cells was significantly inhibited (Figure 1F).

To better investigate the molecular signals modulated by combined romidepsin-IFN treatment we performed RNA-seq analysis. RNA-seq data raw counts values were reported in Table S5. First, unbiased hierarchical clustering of the different transcriptomes using the Pearson's correlation analysis as a similarity metric showed intragroup correlation within untreated and romidepsin-IFN treated MM cells, except for untreated and drug-treated MM1 (Figure 2A). The volcano plot displayed a remarkable increased expression of genes in drug-treated MM cells vs untreated ones since 520 and 360 genes out of the DEGs were up- and down-modulated, respectively (Figure 2B). The top upregulated DEGs by treatment were IFN-induced genes, such as *RSAD2* (Viperin), *IFIT1*, *IFI44L* and the top downregulated DEGs were *TRPM1*, *WFDC1* and *MORC1* (Figure 2C, Table S6). The further hallmark gene set-based enrichment analysis showed the strengthen of romidepsin-IFN combination to up-modulate mainly gene sets linked to inhibition of cell proliferation and chemotaxis, and simultaneously to down-modulate gene sets governing cell cycle and chromatin remodeling (Figure 2D). Specifically, innate immune response, inflammatory response and cytokine-mediated signaling pathway resulted the most positively enriched, whereas the significantly down-regulated gene sets were chromosome segregation, nuclear division and DNA replication (Figure 2E). Further investigation of changes in individual genes revealed drug-driven upmodulation of proapoptotic genes, such as *IRF-1*, *TMFSF10*, *GPX3* and *GADD45A*, many molecules positively linked to apoptosis (*IFIT1*, *IFIT2*, *IFIH1*, *TXNIP*, *ISG15*, *TRIM-21*, *MX1*, *EIF2AK2*, *PNPT1*, *OAS1*) and factors of the IFN-α pathway, along with specific inhibition of negative apoptotic regulators, such as *LEF1*, *BRCA1*, *TOP2A* and *WEE1* (Figure 3A,B). Importantly, drug combination re-established the main signals associated to IFN-γ, such as cell proliferation inhibition, enhancement of antigen presentation and immune response, recently reported to drive the response to immune checkpoint blockade (Figure 3C), and induced a strong down-modulation of several key genes of pathways promoting cancer growth such as G2M checkpoint, Myc and E2F targets (Figure 3D-F).[29] Of note, despite the small

numbers of AXL^high cell lines included in our study, the comparison between AXL^high and MITF^high cells revealed the expected enrichment of MITF^high cells in pigmentation- and proliferation-related genes, such as *DCT*, *MITF*, *MLANA*, *TYRP1*, *SLC7A5*, *CDK2*, along with the impoverishment of genes linked to immune and invasiveness signals, such as *ST8SIA5*, *AXL*, *PTN* and *TAC1* (Figure S3A, Table S7). Of interest, romidepsin-IFN-treated MITF^high cells exhibited strong down-modulation of genes linked to proliferation (*MITF*, *GPM6B*, *TYMS*, *PBK*, *CDK2*), and to EMT (*TRPM1*, *TDRD3*) as well as up-modulation of gene associated to immune signals, such as *IFIT1*, *IFI44L*, *IF16*, *MX1*, *MX2* and *TOX2* (Figure S3B, Table S8), whereas drug-treated AXL^high cells showed up-modulation of an array of immune genes, including *STAT1*, *ISG15*, *OAS3* and *PTX3* (Figure S3C, Table S9). Overall, RNA-seq analysis demonstrated the high capability of romidepsin-IFN treatment to activate genes supporting inhibition of proliferation and activation of antitumor immune response.

3.2 | BRAF-mutated cells resistant to vemurafenib are susceptible to the antitumor effects of romidepsin/IFN treatment

To investigate whether romidepsin/IFN treatment could exert antitumor effects against cells resistant to BRAFi treatment we generated the VEM-resistant MM1-R, MM2-R and MM3-R cell lines, which maintained high cell viability in culture at VEM doses lethal for the parental counterparts (Figure S4). VEM-R cell lines were constantly cultured in the presence of IC50 dose of VEM, which resulted higher for MM3-R cells than the others indicating their elevated acquired resistance (Figures 4A and S4; Table S1).

Since BRAFi resistance develops due to MAPK/ERK pathway reactivation or other mutational patterns may emerge from BRAFi-selective pressure, we searched for possible acquired genetic alterations. *BRAF*-mutated MM1, MM2 and MM3 cells as well as VEM-R derived counterparts were analyzed by parallel sequencing using a panel of 554 genes implicated in cancer development and progression (Table S3). Heterogeneous mutation patterns were found across VEM-R cells and those of MM1-R and MM2-R cells resulted similar to the parental counterparts (Figure 4B, Table S10). In particular, MM1-R and MM1 cells exhibited a similar limited number of mutations distinguished mainly by the homozygosity for the oncogenic V600E change in *BRAF* and for the likely pathogenic C244W substitution in *PTEN*,

---

FIGURE 1 Romidepsin-IFN combination exerts functional and molecular antitumor effects. (A) Direct Sanger sequencing of primary metastatic melanoma cells showing BRAF^V600 mutations. (B) MTS assay of MM cells showing basal cell viability after 24, 48 and 72 hours of culture. Data are expressed as mean ± SD of four independent experiments (***$P < .001$). The absorbance value of SK-Mel-28 after 72 hours of basal proliferation was considered as 100%. (C) Antiproliferative activity of romidepsin (R) and IFN-α2b (I), alone or in combination (RI) evaluated after 48 hours-culture in primary melanoma cells by MTS assay. Data are expressed as mean ± SD of three independent experiments (***$P < .001$; **$P < .01$; *$P < .05$). (D) Blocking of wound healing closure in BRAF^V600 and BRAF^WT MM cells upon RI treatment. Pictures are representative of three independent experiments (×10 magnification). Graphs represent average values of 10 random wound measurements at each time point obtained by ImageJ analysis. (E) MITF/AXL ratio was calculated as ratio of HPRT-normalized MITF and AXL basal relative expression levels obtained by qRT-PCR analysis. (F) Inhibition of MITF and AXL expression in MM cells by RI combined 48 hours-treatment. qRT-PCR data are expressed as ratio of individual gene and HPRT expression and represent the mean ± SD of three independent experiments, ***$P < .001$.

FIGURE 2 Modulation of differentially expressed genes in primary melanoma cells by romidepsin-IFN combined treatment. (A) Heatmap of Pearson's correlation analysis among untreated and RI-treated primary melanoma cells showing high correlation within untreated and drug-treated MM cells, with the only exception of MM1-RI. (B) Volcano plot of modulated genes in primary melanoma cells showing each gene's −log10 (FDR) and log2 fold change with the chosen covariate. Significantly modulated genes (FDR <0.1 and log2 fold change >1) are highlighted in red, whereas down-regulated genes (FDR <0.1 and log2 fold change <−1) are indicated in green. The vertical dashed lines indicate the thresholds for up-regulated and down-regulated genes and the horizontal dashed line represents the FDR threshold. The 100 most statistically significant genes are labeled. (C) Barplot showing the number of DEGs identified with FDR <0.1 and log2 fold change >1/<−1; red and green bar indicate up-modulated and down-modulated DEGs, respectively. (D) Over-representation analysis of significant up-regulated and down-regulated gene sets according to GO Biological Process terms in RI-treated vs untreated primary melanoma cells. Hierarchical clustered of enriched terms were performed according their semantic similarities using Jaccard's similarity index. Dot size is correlated with the number of modulated DEGs of the GO term; dot color shows q-value. (E) Bar plot showing over-representation results values of modulated gene sets according to GO Biological Process terms in RI-treated vs untreated primary melanoma cells. Bars represent the number of DEGs, which belong to a GO term and color scale shows the q-value (FDR) associated with each gene set.
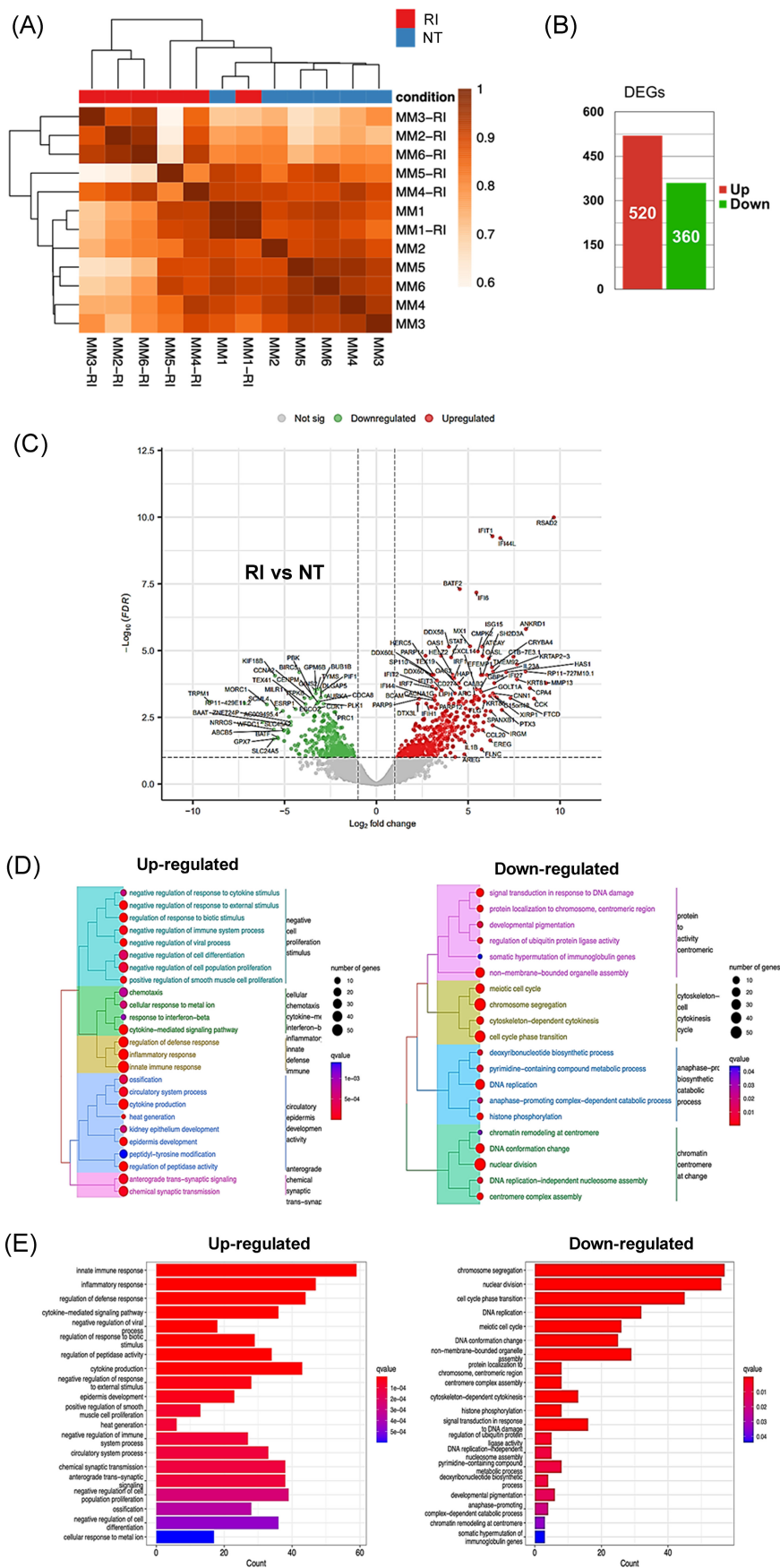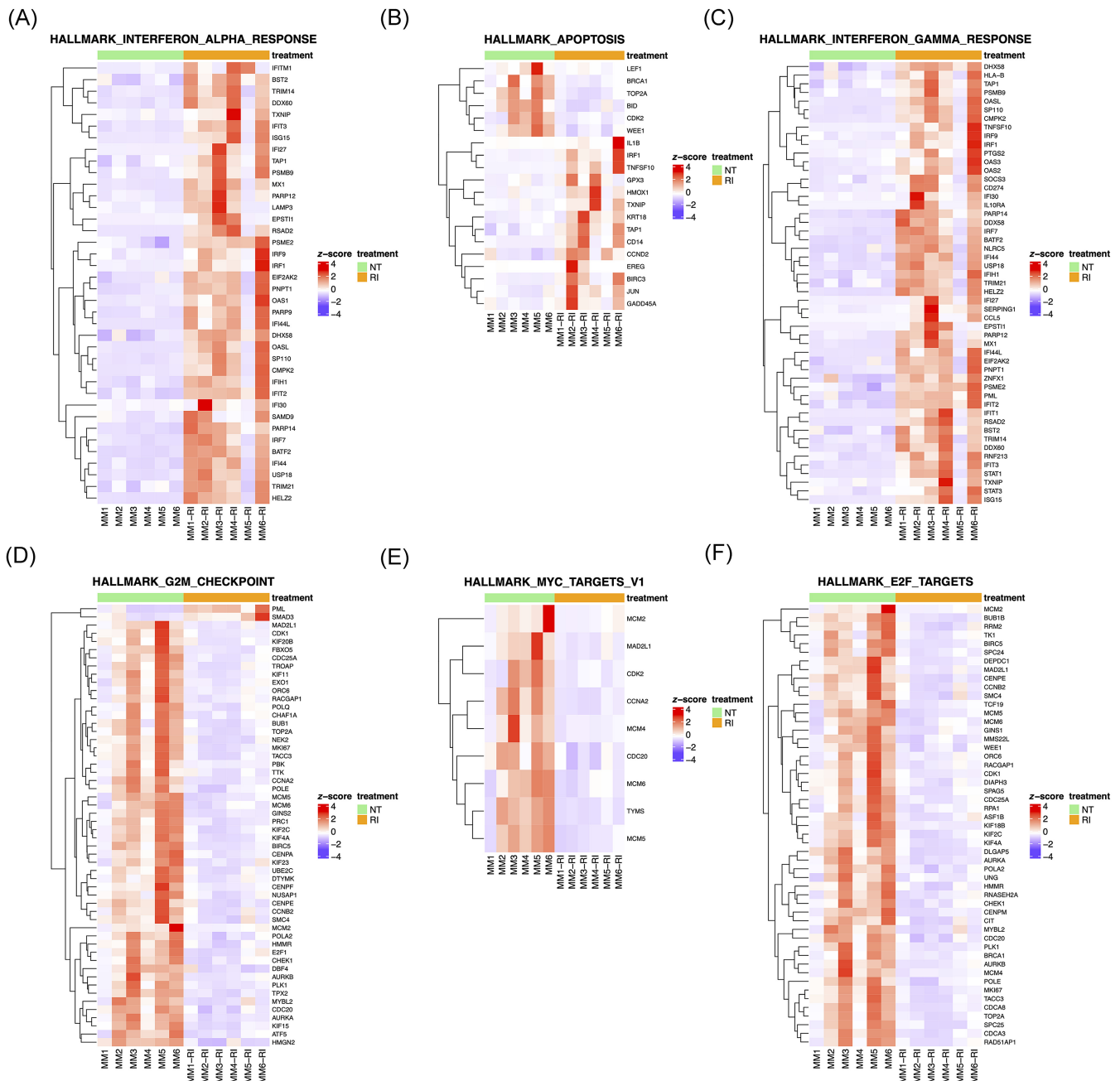
FIGURE 3 Romidepsin-IFN combined treatment modulates genes belonging to specific hallmark pathways. (A-F) Heatmaps displaying Z-score scaled expression values of genes, belonging to modulated MSigDB Hallmark gene signatures according to GSEA results and clustered using Euclidean distance metric, in RI-treated and untreated primary melanoma cells. The color of the grids denotes the enrichment scores of the gene set, with red representing high enrichment and violet representing low enrichment. (A) Hallmark_IFN-alpha response; (B) Hallmark_Apoptosis, (C) Hallmark_IFN-gamma response; (D) Hallmark_G2M-checkpoints; (E) Hallmark_MYC-targets and (F) Hallmark_E2F-targets.

whose loss of function cooperates with activated BRAF to induce metastatic melanoma.[30] MM2-R and MM2 cells displayed a high rate of functionally relevant variants indicative of clonal heterogeneity, with the only significant prevalence of the G170E substitution in *LTK* in VEM-R cells with respect to the parental counterpart. Of note, both MM2-R and MM2 cell lines were clonal for the homozygous pathogenic variants in *PTPRD* and *CDKN2A* as well as for a truncating variant in *MAP2K4/MKK4*, encoding a kinase acting as tumor suppressor in various cancers[31-33] (COSMIC database, https://cancer.sanger.ac.uk/cosmic), and a

previously unreported missense variant (E1695G) in the *CHD5* tumor suppressor gene.[34] Overall, both low-proliferating AXL^high MM1-R and AXL^high MM2-R cells did not show relevant changes in allele proportions compared to their matched parental counterparts, indicating the absence of functional selection during BRAFi treatment driven by mutations. On the contrary, a strong selection was evident for the high-proliferating MITF^high MM3-R cells, compared to parental MM3, as these cells were apparently characterized by a significant enrichment of variants affecting well-known proto-oncogenes and tumor suppressors with role in MAPK
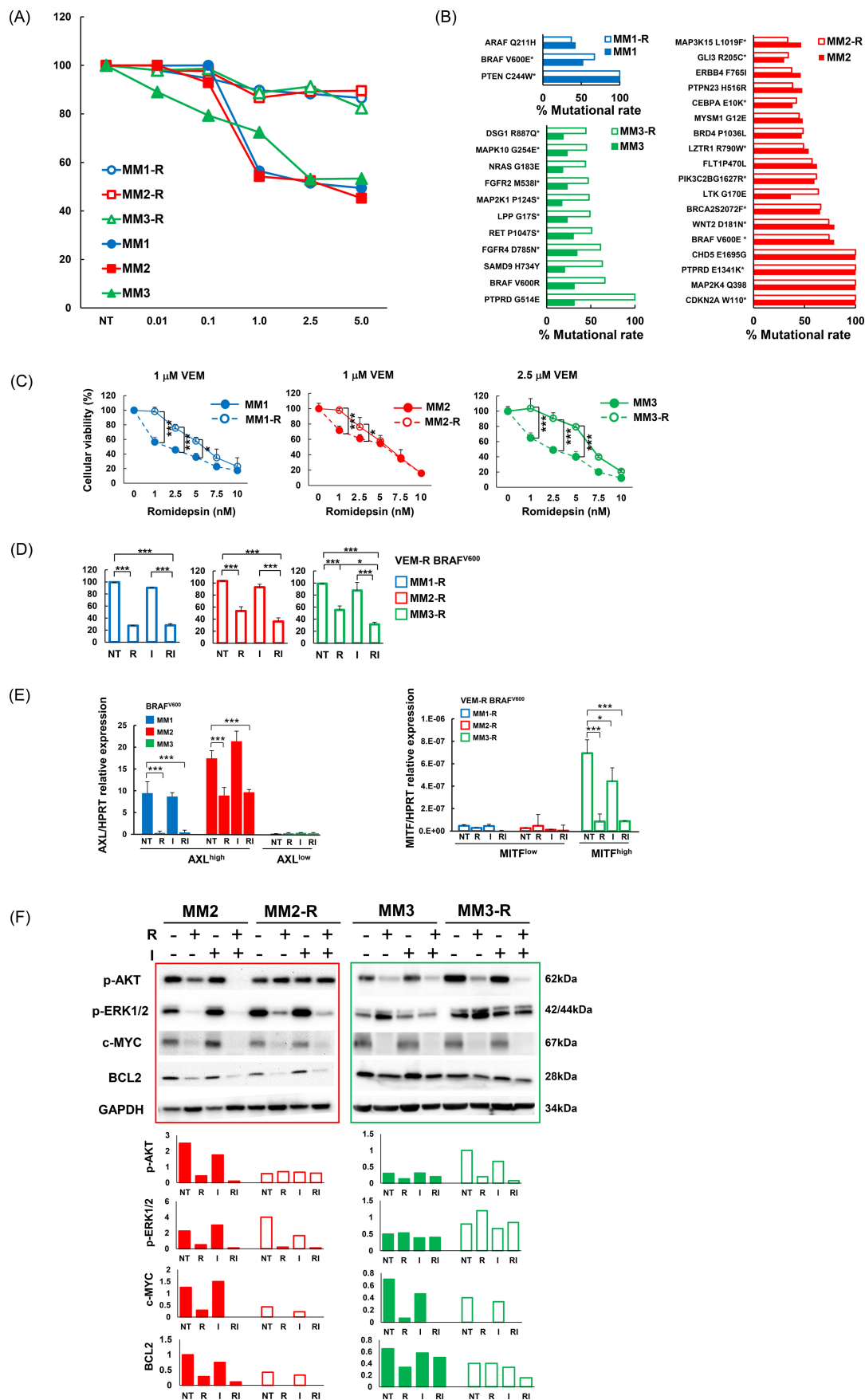
FIGURE 4 Legend on next page.

signaling, such as *PTPRD* (G514E, from 31% to 100% of total reads), *BRAF* (V600R, from 31% to 66%) and *MAP2K1* (P124S, from 17% to 48%), the most common cancer-associated amino acid substitution affecting the MEK1 kinase linked to BRAFi resistance[35] (COSMIC). Of note, MM3-R cells displayed also loss of some variants in selected genes (Figure 4B, Table S10).

Next, VEM-R cells were tested for sensitivity to romidepsin exhibiting dose-dependent decrease of cell viability significantly lower than the parental nonresistant counterparts and full reversion of acquired resistance at the highest drug dose (Figures 4C and S5A). The strong effects of IC20 dose of romidepsin-IFN, or single romidepsin, in arresting VEM-R tumorigenic potential (Figure 4D) were further confirmed by the high frequency of plate-detached nonviable cells, inhibition of long-term cell clonogenic capability and delayed wound healing closure (Figure S5B-D). Similarly to matched parental cells, VEM-R cells displayed basal high MITF or AXL mRNA levels and romidepsin-IFN combined treatment, or single romidepsin, produced a clear-cut down-modulation of *AXL* and *MITF*, where highly expressed (Figure 4E). Of interest, the analysis of p-AKT and p-ERK1/2 levels revealed their heterogeneous activation in VEM-R cells. As compared to the matched parental counterparts, the distinctive traits of AXL[high] MM2-R and MITF[high] MM3-R cells were enhanced basal expression of p-ERK1/2 and p-AKT, respectively, whose levels were sharply down-modulated by romidepsin/IFN treatment, along with c-Myc and Bcl-2. However in both MM2 and MM3 cells as well as their resistant counterpart the Bcl-2/BAX ratio was significantly decreased in Romidepsin/IFN-driven down-modulation of all these molecules was also observed in the parental counterparts, except for p-ERK1/2 in MM3 cells (Figure 4F). Altogether, these data confirm the capability of romidepsin-IFN to silence cellular signals associate to drug-resistance in VEM-R cells.

3.3 | Romidepsin/IFN treatment activates apoptotic/necroptotic cell death pathways in primary BRAF-mutated and VEM-resistant MM cells and increase phagocytosis by DCs along with TIM-3 down-modulation

Next, we demonstrated that combined romidepsin-IFN, and to a lesser extent single romidepsin, induced remarkable cell death in both VEM-R cells and parental counterparts (Figures 5A and S6). The further use of the pan-caspase apoptosis inhibitor Z-VAD and the specific necroptosis inhibitor, necrostatin-1 revealed that romidepsin/IFN was able to induce both apoptosis and necroptosis in both VEM-R and parental cells. Specifically, while the suppression of apoptosis was prevalent in AXL[high] MM2 and MM2-R cells, necroptosis was inhibited mainly in MITF^{high} MM3 cells, particularly in MM3-R cells (Figures 5A and S6). Notably, a strong induction of the production of mitochondrial reactive oxygen species (ROS), which can be correlated immunogenic cell death (ICD) was found,[36] sharply reduced by Z-VAD in MM2/MM2-R cells and by necrostatin-1 in MM3/MM3-R cells (Figure 5B). The higher propensity of MITF[high] MM3 and MM3-R cells to undergo necroptosis following romidepsin-IFN treatment was also confirmed by the induction of pMLKL and RIP1 necroptotic markers as compared to AXL[high] MM2 and MMR-2 (Figure 5C). In addition, in this latter group of cells the basal expression of Bcl-2 was found significantly higher than in the MM3 counterparts whereas basal Bax expression was similar in all tested cells (Figure S7A). Of note, upon RI treatment, AXL[high] MM2 and MMR-2 exhibited down-modulation of Bcl-2 and up-modulation of Bax, confirming the induction of apoptotic cell death whereas MITF[high] MM3 and MM3-R cells showed only up-modulation of Bax, likely accounting for the minor fraction of apoptosis observed in these cells (Figure S7A,B). Importantly, the ICD markers CXCL10, IRF-1 and iNOS and were also increased upon treatment in both AXL[high] and MITF^{high} melanoma cells (Figure S8A). Moreover, a remarkable increase in the expression of PD-L1 was observed (Figure S8B). Finally, AXL[high] and MITF^{high} melanoma cells were found to be negative for HLA-DR expression (Figure S9A). To further evaluate the potential of romidepsin-IFN treatment to induce a strong immune response toward melanoma cells, we concurrently treated with drugs primary CD11c^{+} DCs differentiated from peripheral monocytes, known to be endowed with a high capability in inducing antitumor T cell response, and AXL^{high} and MITF^{high} melanoma cells. Only upon treatment with romidepsin-IFN, DCs were found to express high levels of the activation markers CD80 and CD40, HLA-DR molecule and IL12p40 (Figure 6A-C). Importantly, these DCs were able to engulf with a very high rate drug-treated sensitive and VEM-R cells, undergoing cell death (Figures 6D and S9B). Noteworthy, upon phagocytosis of drug-treated melanoma cells DCs exhibited a sharp down-modulation of the immune checkpoint TIM-3 (Figure 6E).

FIGURE 4 Vemurafenib-resistant primary melanoma cells are highly sensitive to the antitumor effects of romidepsin-IFN in combination. (A) Cell viability of VEM-resistant BRAF[V600]MM cell lines (MM-R) 48 hours-cultured with VEM doses lethal for paired parental cells evaluated by MTS assay. Data are expressed as mean ± SD of three independent experiments (***$P < .001$). (B) Percentage of the mutational rate of MM-R as compared to paired parental counterparts evaluated by NSG analysis. Asterisks mark potential pathogenic variants. (C) Sensitivity to romidepsin of MM-R cells evaluated by MTS assay. Cells were cultured for 48 hours with specific IC50 VEM concentrations and increasing doses of romidepsin. Data are expressed as mean ± SD of three independent experiments (***$P < .001$). (D) Anti-proliferative effects of RI treatment on MM-R cells after 48 hours cultures evaluated by MTA assay. Data are expressed as mean ± SD of three independent experiments (***$P < .001$; *$P < .05$). (E) Inhibition of AXL and MITF transcript by 48 hours-treatment with combined RI evaluated by qRT-PCR. Data are expressed as ratios of individual genes and HPRT and represent the mean ± SD of three independent experiments (***$P < .001$). (F) Inhibition of specific molecules of MAPK and Akt pathways in MM-R cells by 48 hours-RI treatment evaluated by western blot analysis. Densitometry values of the representative blots are reported as relative values normalized on GAPDH.

FIGURE 5 Romidepsin-IFN in combination induces apoptotic/necroptotic cell death and mitochondrial ROS production in primary BRAF-mutated and VEM-resistant melanoma cells. (A) Inhibition by Z-VAD and necrostatin-1 of MM and MM-R cell death induced by 72 hours-RI combined treatment evaluated by flow cytometry after FITC-AnnexinV (AV) and PE-Propidium Iodide (PI) staining to determine the percentage of dead cells (sum of AV+/PI+ +, AV$^+$/PI$^-$ and AV$^-$/PI$^+$ cells). Data are expressed as mean ± SD of four independent experiments (***P < .001; *P < .05). (B) Inhibition of 72 hours-RI treatment-induced mitochondrial ROS production by Z-VAD and necrostatin-1 in MM and MM-R cells. Data are expressed as mean ± SD of four independent experiments (***P < .001; **P < .01, *P < .05). (C) Induction of necroptotic molecules in MM and MM-R cells by 48 hours-RI treatment evaluated by western blot analysis. Densitometry values of the representative blots are reported as bar plots of relative values normalized on GAPDH.
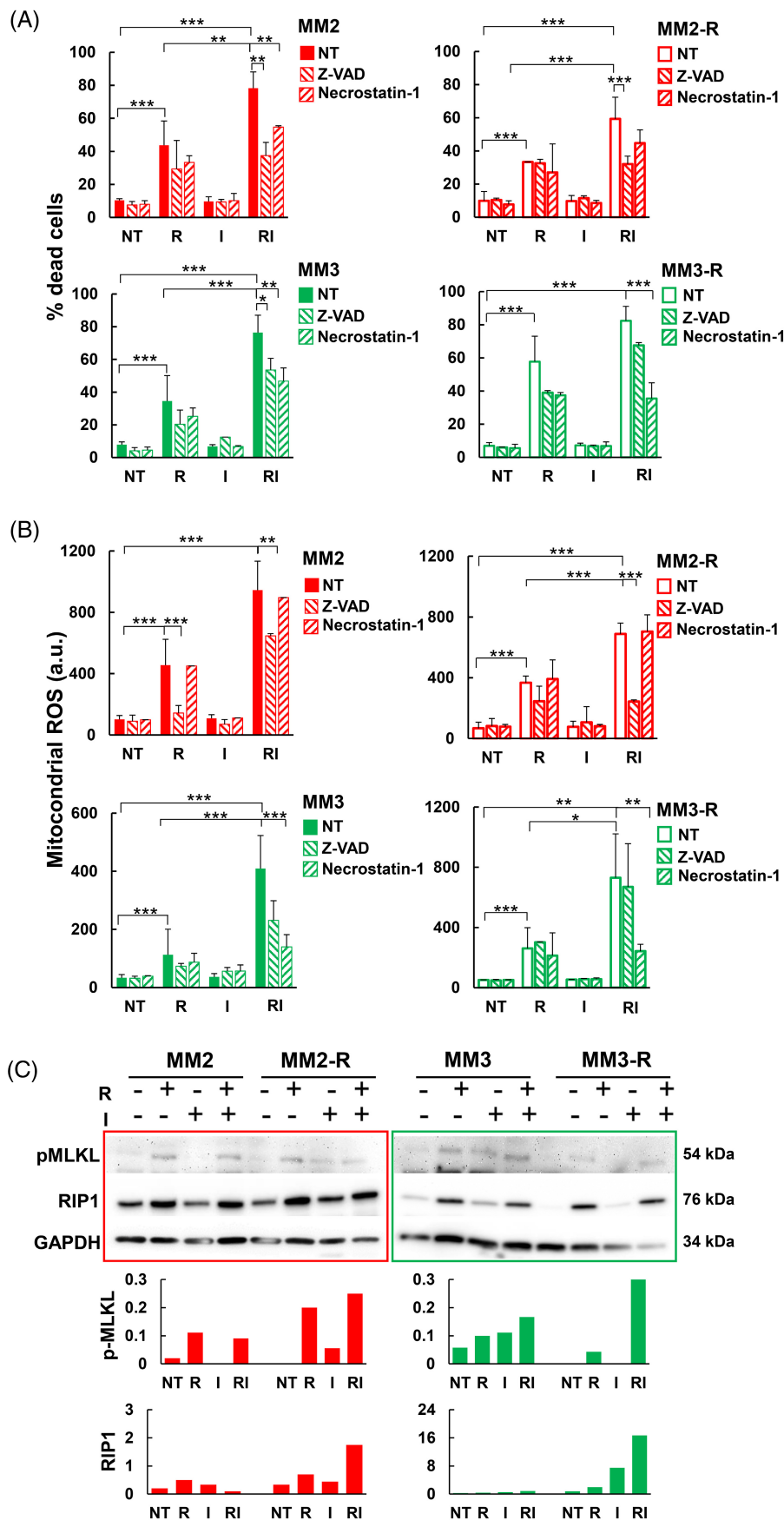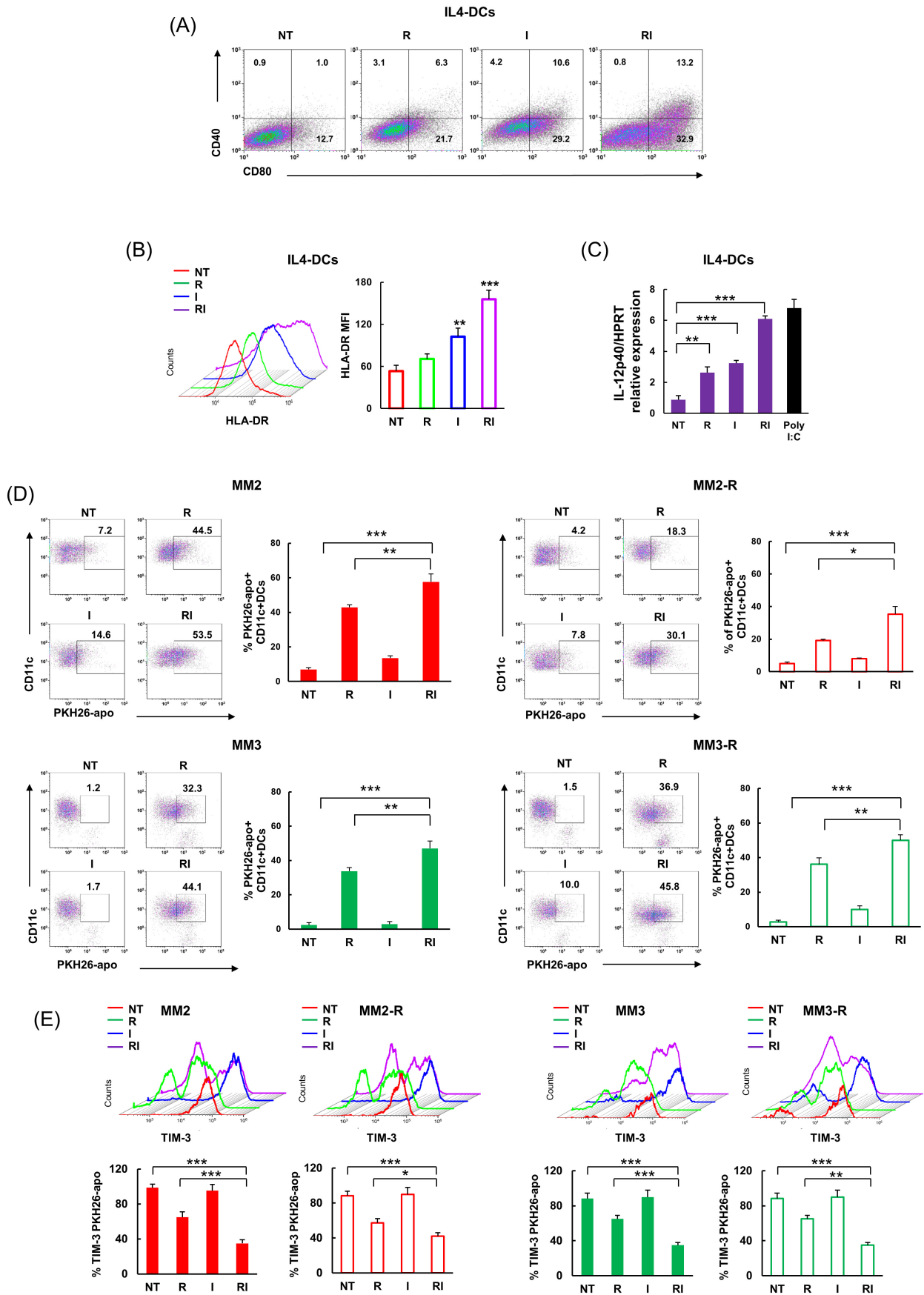
FIGURE 6 Legend on next page.

4 | DISCUSSION

The comprehension of BRAF[V600] dysregulated signaling has led to the development of BRAFi and MEKi. Unfortunately, their clinical use has led to only a transient improvement of clinical outcome due to the development of resistance within 1 year.[2] BRAFi resistance is a complex process shaped by the high heterogeneity and plasticity of TME under the intense drug-driven crosstalk occurring between cancer and noncancer cells. The tumor phenotype plasticity is the core of the well-known phenotype-switch model, characterized by EMT guiding the shift from a proliferative phenotype, distinguished by MITF[high] status, to an invasive one enriched with the most prominent resistance marker AXL[high] but with coexisting MITF^{high} cancer cells.[37,38] Importantly, the dominance of AXL signaling stimulates immune suppression in the TME.[39] In this article, we provide evidence that romidepsin and IFN combination exerts antitumor and immunogenic effects against BRAF-mutated melanoma cells and breaks acquired VEM-resistance of these cells along with the inhibition of MITF/AXL expression.

We performed a deep biological and genetic characterization of six different primary melanoma cell lines, among which MM1, MM2 and MM3 were BRAF[V600] mutated, while MM4, MM5 and MM6 were BRAF[WT]. Regardless the BRAF mutational status, MM3, MM4, MM5 and MM6 cells exhibited high rates of proliferation and migration, whereas MM1 and MM-2 resulted in low proliferating and migrating cells. Accordingly, the former were found MITF[high] and the latter AXL[high]. This finding supports the evidence that MITF/AXL status may be dominant on BRAF mutations to drive the proliferative potential of primary melanoma cells thus suggesting that an early and correct diagnosis of melanoma would largely benefit from a complete knowledge of this parameter.[40]

Recent works have highlighted the potential role of HDACs in melanoma progression.[7,41,42] The epigenetic control of MITF/AXL status has been reported in several types of cancer. MITF[low]-driven melanoma phenotype-switch is associated with activated histone modifications whereas AXL expression under HDAC control is reversed in glioma by combined treatment of AXL and HDAC inhibitors showing potent antitumor effects.[43,44] Of interest, epigenetic driver mutations may shape melanoma immune phenotype by affecting IFN responsiveness and favoring immune evasion thus HDACi showed the ability in promoting the shift to proinflammatory TME,[45,46] and several trials are evaluating the effects of HDAC inhibition in melanoma.[3] In our study, we show that the HDAC class I-selective agent romidepsin, inhibited to the same degree the proliferation of MITF^{high} cells, whereas exerted slightly weaker antiproliferative effects against AXL^{high} cells. Noteworthy, the combination of romidepsin with the immunomodulatory agent IFN resulted in a cooperative antiproliferative effect in all tested MM cells. Specifically, significant suppression of migration and invasion occurred at an equal rate in MITF^{high} cells, as well as in AXL^{high} cells, along with specific inhibition of MITF expression in the former and AXL in the latter group. Romidepsin-IFN treatment sharply determined gene expression reprogramming with the up-modulation of 520 genes and the down-modulation of 360 genes shared by almost all MM cells. Importantly, the most significantly up-modulated genes were associated to immune response signature, such as RSAD2, IFIT1, IFI44L, BATF2 and IFI6, apoptosis, inflammation and IFN pathways while down-modulated genes were linked to cell cycle progression, G2M, Myc and E2F signals.[47] Overall, romidepsin-IFN combination owns the capability to efficiently suppress cellular pathways essential for proliferation and survival, and at once to modulate immune pathways leading on one hand to direct killing of primary melanoma cells and on the other hand to the activation of signals stimulating antitumor immune response.

In the second part of our study, we addressed the main unmet need in melanoma therapy which is the development of an effective treatment for patients failing targeted therapies due to acquired drug resistance. To this end, we generated in vitro VEM-resistant primary melanoma cells starting from primary nonresistant BRAF-mutated melanoma cells. While the mutational assets of MM1-R and MM2-R cells and their parental counterparts were similar, MM3-R cells exhibited a higher mutational rate with respect to the parental MM3. In the former cases, relevant mutations such as C244W substitution in PTEN or variants in PTPRD, CDKN2A, MAP2K4/MKK4 and CHD5 genes, acting to impair tumor suppressor activity, seem not to be associated with acquired-drug resistance. On the contrary, the high rate of mutations acquired during drug-resistance development by MM3-R in key proto-oncogenes and tumor suppressor genes, including MAP2K4/MKK4, suggests their involvement in this event, highlighting the different molecular bases underlying the development of VEM-resistance.[48] The further characterization of VEM-R cells demonstrated that the acquired resistance maintained MITF/AXL status in cell line but led to the differential hyperactivation of pERK1/2 and pAKT in MM2-R and MM3-R, respectively. Noteworthy, these molecules were selectively turned off by romidepsin/IFN treatment along with proliferation arrest and programmed cell death induction.

FIGURE 6 Romidepsin and IFN combined treatment of IL-4 DCs enhances activation markers and uptake of drug-treated MM and MM-R cells—(A,B) 24 hours-drug treated IL4-DCs showing the modulation of the activation markers CD80, CD40 and HLA-DR (C). (C) IL-12p40 production by 24 hours-drug treated IL4-DCs. PolyI:C treatment represents the positive control. Data are indicated as IL12p40/HPRT; expression ratio; after 24 hours bars represent the mean ± SD of three independent experiments; ***P < .001. (D) Phagocytosis rate of CD11c^{+} IL4-DCs co-cultured for 4 hours with PKH26-labeled MM2, MM2-R, MM3 or MM3-R, untreated or 48 hours drug pre-treated stimulating apoptosis; left panels: density plot representative of three independent experiments; right panels: histograms indicating mean ± SD of three independent experiments (***P < .001; **P < .01; *P < .05). (E) Flow cytometric evaluation of TIM-3 expression on double PKH26-apo^{+}CD11c^{+}DCs, representing DC fraction that had performed phagocytosis of melanoma cells; upper panels: histograms representative of three independent experiments; lower panels: % TIM-3 + PKH26-apo + DCs, means ± SD of three independent experiments (***P < .001; **P < .01; *P < .05).

Regarding the ability of HDACi to induce cell death, vorinostat has showed the capability to induce apoptosis selectively in drug-resistant BRAF-mutated melanoma cells leading to tumor regression.[11] Very recently, also romidepsin has been reported to stimulate apoptosis in colon cancer cells, and in combination with anti-PD-1 therapy resulted in a significant inhibition of this tumor by increasing PD-L1 expression in cancer cells.[17] Our data demonstrate that romidepsin-IFN combination was able to induce both apoptosis and necroptosis in both VEM-resistant cells and nonresistant parental counterparts with a prevalence of apoptosis in AXL^{high} cells and necroptosis in MITF^{high} cells, as attested by the selective inhibition of these events by Z-VAD and necrostatin-1 inhibitors and the selective expression of pMLKL and RIP1 proteins. Moreover, high levels of Bcl-2, as we still observed in romidepsin-IFN-treated AXL^{high} cells, have been reported to inhibit necroptosis.[49] Importantly, this treatment was also able to induce high levels of PD-L1 in VEM-R cells, much more effectively than single romidepsin, and to release immunogenic signals, linked to ICD, able to drive their engulfment by DCs that once performed the phagocytosis of cancer cells down-modulated the immune checkpoint TIM-3, suggesting the release of inflammasome activation and ability to present antigen to T cells.[50] In addition, the capability of romidepsin-IFN treatment to elicit a strong antitumor immune response was attested by the activated phenotypic and functional features acquired by drug-treated DCs.[21]

In conclusion, we demonstrate for the first time that romidepsin-IFN treatment induces proliferation arrest and cell death of MITF[high] and AXL[high] VEM-R melanoma cells, activating both apoptosis and necroptosis, inhibiting the activation of pPI3K/AKT and pMAPK/ERK signals, and stimulating immunogenic signals, linked to the antitumor immune response by triggering DCs. The direct and immune-mediated antitumor effects of romidepsin/IFN pave way to be further explored for patients that do not respond to current therapies.

AUTHOR CONTRIBUTIONS

Alessandra Fragale: Conceptualization; methodology; validation; formal analysis; investigation; data curation; writing-original draft preparation; review and editing. **Emilia Stellacci:** Conceptualization; formal analysis; investigation; data curation. **Giulia Romagnoli:** Formal analysis; investigation. **Valerio Licursi:** Software; data curation. **Stefania Parlato:** Formal analysis; investigation. **Irene Canini:** Validation. **Giacomo Remedi:** Software; formal analysis. **Maria Buoncervello:** Investigation. **Paola Matarrese:** Investigation. **Lucia Pedace:** Investigation. **Barbara Ascione:** Investigation. **Simone Pizzi:** Software; data curation. **Marco Tartaglia:** Funding acquisition. **Stefania D'Atri:** Resources. **Carlo Presutti:** Data curation. **Imerio Capone:** Conceptualization; data curation; review and editing. **Lucia Gabriele:** Conceptualization; writing-original draft preparation; review and editing; supervision; project administration; funding acquisition. The work reported in the article has been performed by the authors, unless clearly specified in the text.

ACKNOWLEDGEMENTS

CONFLICT OF INTEREST STATEMENT

The authors declare no conflicts of interest.

DATA AVAILABILITY STATEMENT

The data that support the findings of our study are available from the corresponding author upon reasonable request. The RNA-Seq accompanying this article is available through NCBI's Gene Expression Omnibus (GEO) repository, under accession number GSE221386 located at. https://www.ncbi.nlm.nih.gov/geo/query/acc.cgi?&acc=GSE221386. Other data that support the findings of our study are available from the corresponding authors upon request.

ETHICS STATEMENT

All experiments were conducted in accordance with the Declaration of Helsinki upon approval by Ethics Committee and upon signed informed consent from involved patients.

ORCID

Alessandra Fragale https://orcid.org/0000-0002-0362-1983
Paola Matarrese https://orcid.org/0000-0001-5477-3752
Lucia Gabriele https://orcid.org/0000-0002-1483-866X

REFERENCES

1. Guo W, Wang H, Li C. Signal pathways of melanoma and targeted therapy. *Signal Transduct Target Ther*. 2021;6:424.
2. Caksa S, Baqai U, Aplin AE. The future of targeted kinase inhibitors in melanoma. *Pharmacol Ther*. 2022;239:108200.
3. Hanly A, Gibson F, Nocco S, Rogers S, Wu M, Alani RM. Drugging the epigenome: overcoming resistance to targeted and immunotherapies in melanoma. *JID Innov*. 2022;2:100090.
4. Adams R, Coumbe JEM, Coumbe BGT, et al. BRAF inhibitors and their immunological effects in malignant melanoma. *Expert Rev Clin Immunol*. 2022;18:347-362.
5. Erin N, Grahovac J, Brozovic A, Efferth T. Tumor microenvironment and epithelial mesenchymal transition as targets to overcome tumor multidrug resistance. *Drug Resist Updat*. 2020;53:100715.
6. Arozarena I, Wellbrock C. Phenotype plasticity as enabler of melanoma progression and therapy resistance. *Nat Rev Cancer*. 2019;19:377-391.
7. Ostrowski SM, Fisher DE. Biology of melanoma. *Hematol Oncol Clin North Am*. 2021;35:29-56.
8. Oba J, Woodman SE. The genetic and epigenetic basis of distinct melanoma types. *J Dermatol*. 2021;48:925-939.
9. Emmons MF, Faiao-Flores F, Sharma R, et al. HDAC8 regulates a stress response pathway in melanoma to mediate escape from BRAF inhibitor therapy. *Cancer Res*. 2019;79:2947-2961.
10. Huijberts S, Wang L, de Oliveira RL, et al. Vorinostat in patients with resistant BRAF(V600E) mutated advanced melanoma: a proof of concept study. *Future Oncol*. 2020;16:619-629.
11. Wang L, Leite de Oliveira R, Huijberts S, et al. An acquired vulnerability of drug-resistant melanoma with therapeutic potential. *Cell*. 2018;173:1413-1425.
12. Gallagher SJ, Gunatilake D, Beaumont KA, et al. HDAC inhibitors restore BRAF-inhibitor sensitivity by altering PI3K and survival signalling in a subset of melanoma. *Int J Cancer*. 2018;142:1926-1937.

13. Que Y, Zhang XL, Liu ZX, et al. Frequent amplification of HDAC genes and efficacy of HDAC inhibitor chidamide and PD-1 blockade combination in soft tissue sarcoma. *J Immunother Cancer*. 2021;9:9.

14. Pojani E, Barlocco D. Romidepsin (FK228), a histone deacetylase inhibitor and its analogues in cancer chemotherapy. *Curr Med Chem*. 2021;28:1290-1303.

15. Paillas S, Then CK, Kilgas S, et al. The histone deacetylase inhibitor romidepsin spares normal tissues while acting as an effective radiosensitizer in bladder tumors in vivo. *Int J Radiat Oncol Biol Phys*. 2020;107:212-221.

16. Patel RP, Thomas JR, Curt KM, et al. Dual inhibition of histone deacetylases and the mechanistic target of rapamycin promotes apoptosis in cell line models of uveal melanoma. *Invest Ophthalmol Vis Sci*. 2021;62:16.

17. Shi Y, Fu Y, Zhang X, et al. Romidepsin (FK228) regulates the expression of the immune checkpoint ligand PD-L1 and suppresses cellular immune functions in colon cancer. *Cancer Immunol Immunother*. 2021;70:61-73.

18. Waldmann TA. Cytokines in cancer immunotherapy. *Cold Spring Harb Perspect Biol*. 2018;10:a028472.

19. Levati L, Alvino E, Pagani E, et al. Altered expression of selected microRNAs in melanoma: antiproliferative and proapoptotic activity of miRNA-155. *Int J Oncol*. 2009;35:393-400.

20. Lacal PM, Failla CM, Pagani E, et al. Human melanoma cells secrete and respond to placenta growth factor and vascular endothelial growth factor. *J Invest Dermatol*. 2000;115:1000-1007.

21. Fragale A, Romagnoli G, Licursi V, et al. Antitumor effects of epidrug/IFNalpha combination driven by modulated gene signatures in both colorectal cancer and dendritic cells. *Cancer Immunol Res*. 2017;5:604-616.

22. Motta M, Fasano G, Gredy S, et al. SPRED2 loss-of-function causes a recessive Noonan syndrome-like phenotype. *Am J Hum Genet*. 2021;108:2112-2129.

23. Motta M, Pannone L, Pantaleoni F, et al. Enhanced MAPK1 function causes a neurodevelopmental disorder within the RASopathy clinical spectrum. *Am J Hum Genet*. 2020;107:499-513.

24. Dobin A, Davis CA, Schlesinger F, et al. STAR: ultrafast universal RNA-seq aligner. *Bioinformatics*. 2013;29:15-21.

25. Anders S, Pyl PT, Huber W. HTSeq—a python framework to work with high-throughput sequencing data. *Bioinformatics*. 2015;31:166-169.

26. Huber W, Carey VJ, Gentleman R, et al. Orchestrating high-throughput genomic analysis with Bioconductor. *Nat Methods*. 2015;12:115-121.

27. Ashburner M, Ball CA, Blake JA, et al. Gene ontology: tool for the unification of biology. *Nat Genet*. 2000;25:25-29.

28. Buoncervello M, Romagnoli G, Buccarelli M, et al. IFN-alpha potentiates the direct and immune-mediated antitumor effects of epigenetic drugs on both metastatic and stem cells of colorectal cancer. *Oncotarget*. 2016;7:26361-26373.

29. Grasso CS, Tsoi J, Onyshchenko M, et al. Conserved interferon-gamma signaling drives clinical response to immune checkpoint blockade therapy in melanoma. *Cancer Cell*. 2020;38(500-15):e3.

30. Dankort D, Curley DP, Cartlidge RA, et al. Braf(V600E) cooperates with Pten loss to induce metastatic melanoma. *Nat Genet*. 2009;41:544-552.

31. Walia V, Prickett TD, Kim JS, et al. Mutational and functional analysis of the tumor-suppressor PTPRD in human melanoma. *Hum Mutat*. 2014;35:1301-1310.

32. Iqbal B, Masood A, Lone MM, Lone AR, Dar NA. Polymorphism of metastasis suppressor genes MKK4 and NME1 in Kashmiri patients with breast cancer. *Breast J*. 2016;22:673-677.

33. Xue Z, Vis DJ, Bruna A, et al. MAP3K1 and MAP2K4 mutations are associated with sensitivity to MEK inhibitors in multiple cancer models. *Cell Res*. 2018;28:719-729.

34. Baykara O, Tansarikaya M, Bulut P, Demirkaya A, Buyru N. CHD5 is a potential tumor suppressor in non small cell lung cancer (NSCLC). *Gene*. 2017;618:65-68.

35. Van Allen EM, Wagle N, Sucker A, et al. The genetic landscape of clinical resistance to RAF inhibition in metastatic melanoma. *Cancer Discov*. 2014;4:94-109.

36. Xu Z, Xu J, Sun S, et al. Mecheliolide elicits ROS-mediated ERS driven immunogenic cell death in hepatocellular carcinoma. *Redox Biol*. 2022;54:102351.

37. Pedri D, Karras P, Landeloos E, Marine JC, Rambow F. Epithelial-to-mesenchymal-like transition events in melanoma. *FEBS J*. 2022;289:1352-1368.

38. Sala M, Allain N, Moreau M, et al. Discoidin domain receptor 2 orchestrates melanoma resistance combining phenotype switching and proliferation. *Oncogene*. 2022;41:2571-2586.

39. Ludwig KF, Du W, Sorrelle NB, et al. Small-molecule inhibition of Axl targets tumor immune suppression and enhances chemotherapy in pancreatic cancer. *Cancer Res*. 2018;78:246-255.

40. Davis LE, Shalin SC, Tackett AJ. Current state of melanoma diagnosis and treatment. *Cancer Biol Ther*. 2019;20:1366-1379.

41. Diener J, Baggiolini A, Pernebrink M, et al. Epigenetic control of melanoma cell invasiveness by the stem cell factor SALL4. *Nat Commun*. 2021;12:5056.

42. Comito F, Pagani R, Grilli G, Sperandi F, Ardizzoni A, Melotti B. Emerging novel therapeutic approaches for treatment of advanced cutaneous melanoma. *Cancers (Basel)*. 2022;14:14.

43. Verfaillie A, Imrichova H, Atak ZK, et al. Decoding the regulatory landscape of melanoma reveals TEADS as regulators of the invasive cell state. *Nat Commun*. 2015;6:6683.

44. Meel MH, de Gooijer MC, Metselaar DS, et al. Combined therapy of AXL and HDAC inhibition reverses mesenchymal transition in diffuse intrinsic pontine glioma. *Clin Cancer Res*. 2020;26:3319-3332.

45. Li J, Wang W, Zhang Y, et al. Epigenetic driver mutations in ARID1A shape cancer immune phenotype and immunotherapy. *J Clin Invest*. 2020;130:2712-2726.

46. Knox T, Sahakian E, Banik D, et al. Selective HDAC6 inhibitors improve anti-PD-1 immune checkpoint blockade therapy by decreasing the anti-inflammatory phenotype of macrophages and down-regulation of immunosuppressive proteins in tumor cells. *Sci Rep*. 2019;9:6136.

47. Matthews HK, Bertoli C, de Bruin RAM. Cell cycle control in cancer. *Nat Rev Mol Cell Biol*. 2022;23:74-88.

48. Awada G, Neyns B. Melanoma with genetic alterations beyond the BRAFV600 mutation: management and new insights. *Curr Opin Oncol*. 2022;34:115-122.

49. Shi CS, Kehrl JH. Bcl-2 regulates pyroptosis and necroptosis by targeting BH3-like domains in GSDMD and MLKL. *Cell Death Discov*. 2019;5:151-164.

50. Dixon KO, Tabaka M, Schramm MA, et al. TIM-3 restrains anti-tumour immunity by regulating inflammasome activation. *Nature*. 2021;595:101-106.

SUPPORTING INFORMATION

Additional supporting information can be found online in the Supporting Information section at the end of this article.

B-cell malignancies - A new knowledge hub on the latest research in therapeutic advances

EDUCATIONAL CONTENT AVAILABLE ON THE HUB:

- **On-demand Webinars - earn CME credit**
- **Infographics**
- **Patient Case Studies**
- **Currated Research Articles**
  ...and much more

VISIT KNOWLEDGE HUB TODAY

WILEY